IEEE Access
Multidisciplinary | Rapid Review | Open Access Journal

Received June 12, 2020, accepted July 1, 2020, date of publication July 6, 2020, date of current version July 17, 2020.

Digital Object Identifier 10.1109/ACCESS.2020.3007162

3D Layout of Interdigital Transducers for High Frequency Surface Acoustic Wave Devices

JUNYAO SHEN[1], JINGTING LUO[2], SULEI FU[1], RONGXUAN SU[1], WEIBIAO WANG[3], FEI ZENG[1], CHENG SONG[1], (Member, IEEE), AND FENG PAN[1]

[1]Key Laboratory of Advanced Materials (MOE), School of Materials Science and Engineering, Tsinghua University, Beijing 100084, China
[2]Shenzhen Key Laboratory of Advanced Thin Films and Applications, College of Physics and Optoelectronic Engineering, Shenzhen University, Shenzhen 518060, China
[3]SHOULDER Electronics Limited, Wuxi 214124, China

Corresponding author: Feng Pan (panf@mail.tsinghua.edu.cn)

This work was supported by the National Key Research and Development Program of China under Grant 2016YFB0402700.

ABSTRACT The development of mobile communication sets higher demands on high frequency surface acoustic wave (SAW) devices. The layout of interdigital transducers (IDT) in SAW devices is in plane and the traditional methods of improving frequency for SAW devices are the increase of acoustic velocity and the reduction of wavelength. However, these methods have a limit due to the limited acoustic velocity and the photolithography limit. This work proposes a new way for the development of high frequency SAW devices by redesigning the layout of IDT in three dimensions (3D). The set of IDTs is split into two layers, i.e. the ground electrodes on one layer and the signal electrodes on the other layer. This 3D layout of IDTs dramatically narrows the horizontal gap between two adjacent electrodes, which can significantly increase the frequency. The frequency and the electromechanical coupling factor (K^2) of the four structures of SAW devices with the 3D layout of IDTs were studied by the finite element method (FEM). The results show that the frequency can be doubled under the same critical resolution of lithography due to the shortening of wavelength, and the 3D layout of IDTs is available for SAW devices based on piezoelectric thin film or piezoelectric single crystal. This work develops a new alternative to increase the working frequency of SAW devices.

INDEX TERMS High frequency, interdigital transducer, surface acoustic wave, three-dimensional layout.

I. INTRODUCTION

Surface acoustic wave (SAW) devices have been widely used in the field of communication system, microfluidic and sensor. [1]–[7] With the rapid development of mobile communication technology, especially the emergency of the 5th generation (5G) wireless system has promoted the frequency range into Sub-6 and even millimeter Wave, which demands a large number of high frequency filters and duplexers. Hence, many researchers have devoted into a serial of innovative devices with high frequency and good performance. [8], [9] Bulk acoustic wave (BAW) devices whose frequency is dependent on the thickness of the piezoelectric layer can be utilized in high-frequency applications. [10]–[15] But in order to achieve a high quality (Q) factor, the piezoelectric layer cannot be too thin and the fabrication techniques are elaborate, resulting in the limited frequency and high cost. Lamb wave devices which combine the strengths of SAW devices and BAW devices have been the hot area of research in recent years [16]–[21], but the process flow of fabrication is even more complicated than that of BAW devices. Aiming at lowering the cost, many researchers are committed to the study of high frequency SAW devices.

Generally, using wafers with high acoustic propagating velocities and shrinking the period of interdigital transducers (IDT) are two ways to improve the frequency of SAW devices. Recently, AlN thin film has got much attention because it has higher phase velocity (over 5000 m/s) compared to other piezoelectric thin films. [22]–[29] Moreover, it can be deposited on substrates with high phase velocity, such as diamond and SiC, resulting a great candidate for high frequency SAW devices. [30]–[32] The frequency of the device based on AlN/diamond structure reached 5 GHz [33], while a Sezawa wave filter based on ZnO/SiC structure with the center frequency of 6.8 GHz was prepared successfully in our previous work [34]. Longitudinal leaky

The associate editor coordinating the review of this manuscript and approving it for publication was Jenny Mahoney.

surface acoustic wave (LLSAW) is also an option for high frequency devices. [35], [36]

Nevertheless, these conventional methods to improve the frequency of SAW devices have a limit due to the limited acoustic velocity and the photolithography limit. For example, since the layout of IDT in SAW devices is in plane, the period of IDT cannot be prepared into a very small level because of the photolithography limit, the preparation cost and the power durability. This stimulates us to explore a new solution to increase SAW devices frequency. In this paper, we introduce three-dimensional (3D) design into IDTs of SAW devices and demonstrate a 3D layout of IDTs in order to further reduce its wavelength. The IDTs are separated into two layers, i.e. the ground electrodes on one layer and the signal electrodes on the other layer, and thus the gap between electrodes in either part of IDTs can be much smaller, which narrows the wavelength significantly. The devices with this 3D layout of IDTs have much higher frequencies under the same critical resolution of lithography.

II. SIMULATION DETAILS

Four structures with the 3D layout of IDTs, as shown in Fig. 1(a)-1(d), are designed. This work, for the first time, redesigns the layout of IDTs by splitting a set of IDTs into two layers, i.e. the ground electrodes on one layer and the signal electrodes on the other layer. Fig. 1(e) shows the detail of IDTs. The first layer of IDTs is embedded inside either the SiO_2 layer or the piezoelectric layer, while the second layer of IDTs is on the top of the surface. In Fig. 1, the 1st layer of IDTs is connected as the signal input and the 2nd layer to the ground. In fact, the electrical connection of these two layers can be reversed. The horizontal gap between two adjacent electrodes with different polarities is g_1, while g_2 stands for the gap of electrodes with the same polarity. If we note the width of each electrode as d, then there is an equation as follows.

$$g_2 = d + 2 \times g_1 \tag{1}$$

These sizes are the key to narrow the wavelength (λ) and increase the frequency.

$$\lambda = 2 \times (d + g_1) \tag{2}$$

The first high frequency structure with the 3D layout of IDTs based on piezoelectric thin film, e.g. zinc oxide, is composed of a piezoelectric thin film, SiO_2 and a substrate, as shown in Fig. 1(a). Fig. 1(b) depicts another structure for piezoelectric thin film, where the piezoelectric thin film is sandwiched between SiO_2 layer and the substrate. The structure shown in Fig. 1(c) is formed by SiO_2/ piezoelectric crystal substrate. The 1st layer of IDTs in the first three structures are all covered by SiO_2 layer because SiO_2 thin film grows compactly both on and between the electrodes and also plays a vital role in temperature compensation for SAW devices. The design in Fig. 1(d) has the simplest structure which directly buries the 1st layer of IDTs into the piezoelectric crystal without using SiO_2 layer.

This work theoretically studies all the four structures by the finite element method (FEM) via COMSOL Multiphysics software. All the structures in COMSOL only has one period with periodic boundaries for side faces and specific materials are modelled for each structure. Al electrode/ c-ZnO/ SiO_2 (Al electrode)/ Si(100) substrate, Al electrode/ SiO_2 (Al electrode)/ c-ZnO/ Si(100) substrate, Al electrode/ SiO_2 (Cu electrode)/ 15°Y-X $LiNbO_3$ substrate, Al electrode/ (Cu electrode) 15°Y-X $LiNbO_3$ substrate, respectively standing for the structures in Fig.1(a)-1(d), are systematically simulated. 15°Y-X $LiNbO_3$ is chosen because SAW devices based on 15°Y-X $LiNbO_3$ possess large value of the electromechanical coupling factor (K^2). [37]

The material constants cited from references [38]–[40] are given in the global coordinate system (X, Y, Z) in COMSOL. To achieve the orientation of 15°Y-X for $LiNbO_3$ substrate, this work defines the Euler angle of (0, 75°, 0), according to the rule of COMSOL, while it is unnecessary to set the rotated coordinate systems for the structures in Fig. 1(a) and 1(b). Two dimensional model is used for the simulation of the structures in Fig. 1(a) and 1(b) because the displacement in the transverse direction is negligible, while the other two designs in Fig. 1(c) and 1(d) are built based on the three-dimension models.

Electrically grounded boundary condition and terminal condition are set respectively for one of the electrodes in each model. In the simulation, the wavelength is controlled by changing three key parameters g_1, g_2 and d, and the height of each electrode is adjusted. The thickness of each thin film layer is also an important factor which greatly influences the performance of SAW devices. The ratio of the thickness (h) to the wavelength (λ) depicts the change of the thickness in this work.

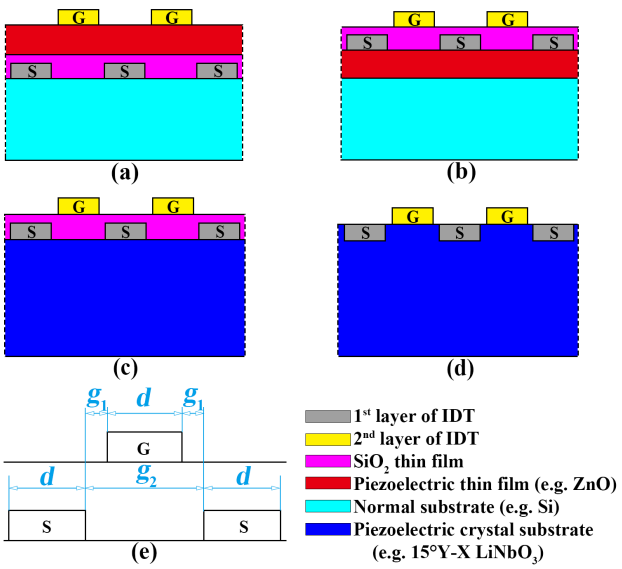

FIGURE 1. Schematics showing the design of the first structure (a), the second structure (b), the third structure (c), the fourth structure (d) with the 3D layout of IDTs (e).

The frequency (f) is defined as:

$$f = (f_r + f_a)/2 \tag{3}$$

where f_r and f_a are the resonance frequency and the anti-resonance frequency, respectively.

The electromechanical coupling factor (K^2) is calculated from the following equation [41].

$$K^2 = \frac{\pi f_r/(2f_a)}{\tan[\pi f_r/(2f_a)]} \tag{4}$$

This 3D layout of IDTs brings an electric field with perpendicular component which activates the bulk wave. If the bulk wave is not controlled, it propagates inside the whole structure and does harm to the signal because of energy dissipation. An IDT-modulation method, which is to prepare two layers of IDTs with different thicknesses and even with different materials, is proposed to neutralize the effect from perpendicular component of the electric field. Simulation results show that the bulk wave can be suppressed when the thicknesses and materials of the two layers of IDTs are different and match up with each other. Therefore, in the second, third and fourth structures, this IDT-modulation method is adopted to suppress the bulk wave and ensure the quality of signals. The first structure is special. When silicon substrate is applied as the normal substrate in Fig. 1, piezoelectric layer/ SiO_2/ Si structure is similar to Incredible High-performance SAW (I.H.P.SAW) devices [42] and solidly mounted resonator (SMR) [43] which has the ability to confine acoustic wave, to some extent. Simulation results show that the bulk wave can be confined and the signal is as great as conventional SAW devices only if the thicknesses of the piezoelectric layer and SiO_2 are proper. In this article, in order to show the results of the original first structure and the confining effect from SiO_2/Si double layer, the IDTs in the first structure are not modulated like the other three structures, but the approach of IDTs modulation can also be used in the first structure to ensure the quality of all the signals.

Fig. 2 shows typical admittance curves of the models designed for the four structures in Fig. 1, respectively. The insets in Fig. 2 display the deformation shape when the SAW is excited. For the structures based on ZnO thin film, the signal of the Sezawa mode wave is utilized, while the structures based on 15°Y-X $LiNbO_3$ are the shear-horizontal (SH) wave. In Fig. 2(a) and 2(b), spurious signals can be observed. The signal at about 5 GHz in Fig. 2(a) and 2(b) comes from 0^{th} Rayleigh wave and that at about 9.5 GHz in Fig. 2(a) comes from 1^{st} Rayleigh wave. The admittance ratio (AR) [44] is calculated and shown in Fig. 2, which is defined as:

$$AR = 20\log_{10}|Y_r/Y_a| \tag{5}$$

where Y_r is the admittance at resonance frequency and the Y_a is the admittance at anti-resonance frequency.

The SAW in every structure is excited by the horizontal component of the electric field. In the first structure, the electric field penetrates the ZnO and SiO_2 layer, while the electric field in the second structure mostly focuses on the surface of the structure. Generally, the proportion of the horizontal component in the second structure is higher than that in the first structure. The electric field in the third structure is in the SiO_2 layer and on the surface of the $LiNbO_3$ substrate, while it only focuses on the surface of the $LiNbO_3$ substrate in the fourth structure. More energy can be converted by the $LiNbO_3$ substrate in the fourth structure, so the value of K^2 is larger which can be obviously seen in Fig. 2(c) and (d).

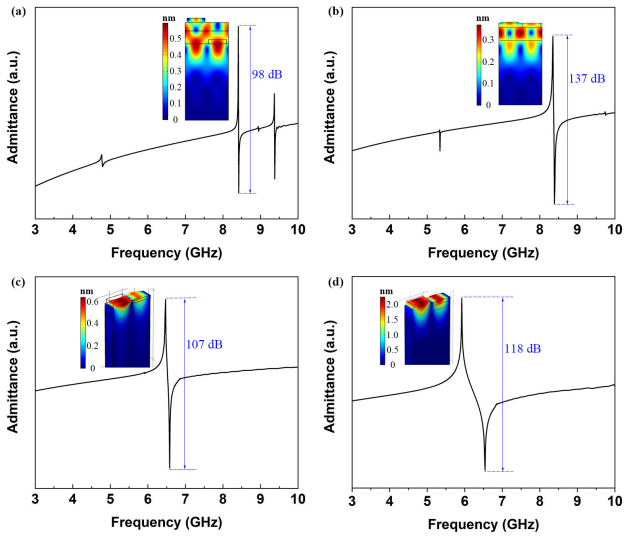

FIGURE 2. Typical admittance curves and corresponding deformation shapes (antisymmetric state) of (a) the first structure, (b) the second structure, (c) the third structure, (d) the fourth structure.

III. RESULTS AND DISCUSSION

A. SIMULATION OF STRUCTURES BASED ON PIEZOELECTRIC THIN FILM

Fig. 3 shows the calculated f and K^2 dispersion patterns of the Sezawa mode wave propagating in the structure which is depicted in Fig. 1(a). In this part of simulation, the width of electrode d is fixed as 250 nm and the height is 60 nm, while the gap g_1 is altered to study the influence of wavelength on the value of f and K^2. Fig. 3(a) and (b), 3(c) and (d), 3(e) and (f), 3(g) and (h) respectively show the f and K^2 dispersion patterns of the wave in the models with g_1 of 150 nm, 100 nm, 50 nm, 10 nm. As mentioned in Section II, the IDTs in this structure are not modulated, so only the structures with $h(ZnO)/\lambda$ of 0.2 and $h(SiO_2)/\lambda$ of 0.3 or 0.4 confine the bulk wave. Under the conditions of other thicknesses, the signal is not as good as conventional SAW devices because of synchronous bulk wave generation. But it does not influence the study about the characteristics of the Sezawa mode wave and it can be solved by IDT-modulation method.

In Fig. 3(c)-(f), several points are omitted because the ZnO and SiO_2 layer are so thin that the signals are weak and not actually valuable in these cases. When the wavelength is 520 nm and $h(SiO_2)/\lambda$ equals 0.1, the thickness of SiO_2 is 52 nm and smaller than that of IDTs. This situation does not meet the design shown in Fig. 1(a), so Fig. 3(g) and (h) only have

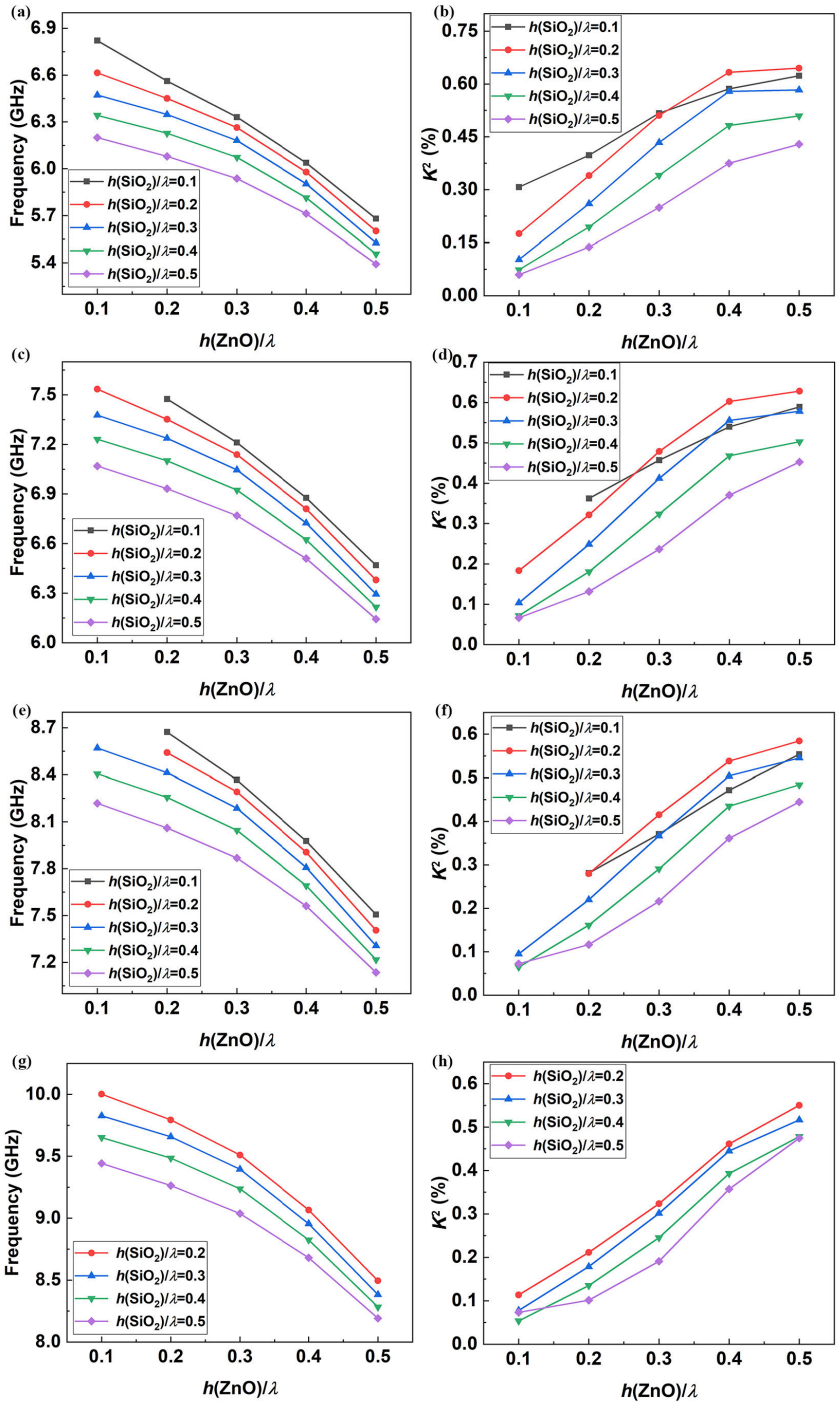

FIGURE 3. Frequency (a, c, e, g) and K^2 (b, d, f, h) as functions of the thicknesses of ZnO and SiO_2 in the first structure with the wavelength of (a, b) 800 nm, (c, d) 700 nm, (e, f) 600 nm, (g, h) 520 nm.

four lines. The frequency increases sharply with the decrease of g_1 because smaller g_1 shortens the wavelength. g_1 does not have a significant effect on the K^2.

The dispersion patterns of the frequency in Fig. 3(a), 3(c), 3(e) and 3(g) exhibit the same trend. The frequency decreases monotonically with the increase of $h(\mathrm{ZnO})/\lambda$ or $h(\mathrm{SiO_2})/\lambda$ due to the smaller phase velocities of ZnO thin film and SiO_2 thin film compared to that of Si substrate. The K^2 has a relatively large value when the ZnO thickness is larger, as shown in Fig. 3(b), 3(d), 3(f) and 3(h), because ZnO thin film is the only layer with piezoelectricity in this structure. Generally, the calculated K^2 rises with decreasing normalized thickness

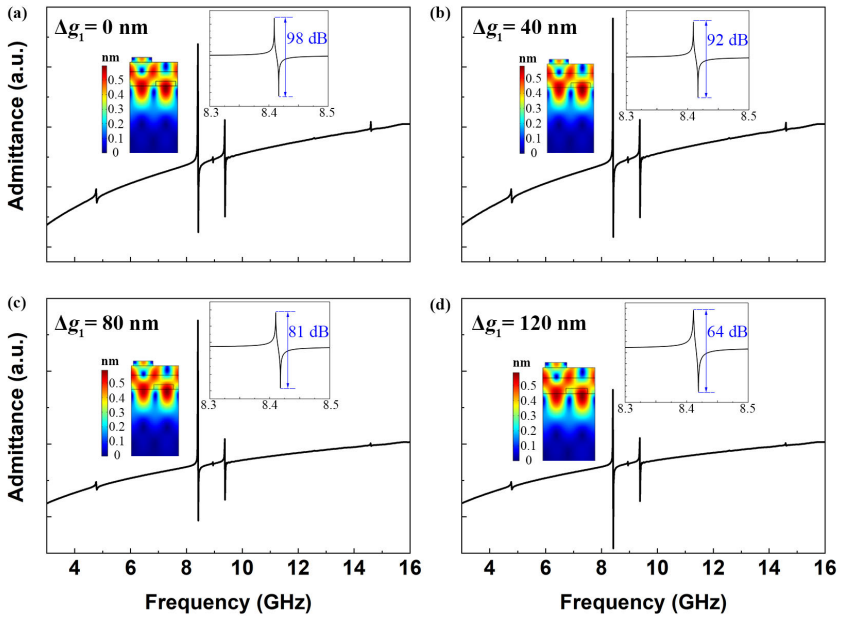

FIGURE 4. Global and local admittance curves and corresponding deformation shapes (antisymmetric state) of the first structure with h(ZnO)/λ of 0.2, h(SiO_2)/λ of 0.3, g_1 of 50 nm, d of 250 nm and (a) Δg_1 of 0 nm, (b) Δg_1 of 40 nm, (c) Δg_1 of 80 nm, (d) Δg_1 of 120 nm.

of the SiO_2 thin film because enlarging the thickness of SiO_2 reduces the proportion of the vibration inside the ZnO layer by the large. In the meantime, the proportion of the vibration inside the ZnO/SiO_2 bilayer increases with the increase of the SiO_2 thickness. So in some special cases, the proportion of the vibration inside the ZnO layer becomes larger when the SiO_2 layer is thicker, then the variation tendency of K^2 is different. Therefore, analyzed in more detail, when the value of h(ZnO)/λ is near 0.4, the value of K^2 increases until the SiO_2 thickness reaches 0.2λ, but then decreases when the SiO_2 thickness is increased further. The maximum frequency of this structure can reach 10 GHz when h(ZnO)/λ equals 0.1, h(SiO_2)/λ equals 0.2, g_1 equals 10 nm and d equals 250 nm. And even the minimum value of frequency is still larger than 5 GHz. Therefore, the 3D layout of IDTs effectively improves the frequency.

Our design of the 3D layout of IDTs is an ideal situation, but the overlay exposure may not be so precise in the practical device-making process. For example, if the purpose is to prepare devices with g_1 of 50 nm and d of 250 nm, the left side g_1 in Fig. 1(e) of the practical device may be 10 nm and the right side g_1 may be 90 nm. Therefore, this work investigates the performance of devices when there is a position offset of IDTs.

So as to measure the value of the position offset, Δg_1 is defined as the difference between the left side g_1 and the right side g_1. The ideal situation is the structure with h(ZnO)/λ of 0.2, h(SiO_2)/λ of 0.3, g_1 of 50 nm, d of 250 nm and Δg_1 of 0, whose signal, deformation shape and admittance ratio are shown in Fig. 4(a). Fig. 4(b)-4(d) show the simulation results of the structures which have position offsets. The spurious waves at about 5 GHz and 9.5 GHz are 0^{th} Rayleigh wave and 1^{st} Rayleigh wave, respectively. When the offset of the 2^{nd} layer of IDT is 20 nm, i.e. Δg_1 equals 40 nm, the signal is almost same as the ideal situation and the admittance ratio is 92 dB which is slightly less than the ideal situation 98 dB, as shown in Fig. 4(b). The device with Δg_1 of 80 nm is still exploitable even if the peaks of the signal are not as sharp as those in the ideal situation and the admittance ratio becomes 81 dB, as shown in Fig. 4(c). An extreme situation in which Δg_1 equals 120 nm is also considered. A model with left g_1 of –10 nm and right g_1 of 110 nm, which means that the two layers of IDTs partially overlap in the vertical direction, is built and studied. Fig. 4(d) shows that the Sezawa mode wave is still excited successfully and the wave form is as good as the former ones. The signal becomes less sharp, resulting in a lower quality factor and a lower admittance ratio of 64 dB, so this extreme situation should better be avoided. Therefore, the first structure shown in Fig. 1(a) has tolerance for the precision of the overlay exposure.

The second structure as shown in Fig. 1(b) is also based on piezoelectric thin film. Although the 2^{nd} layer of IDT in this structure isn't directly attached to the piezoelectric layer, there is still electric field that excites the acoustic wave. The thickness of the SiO_2 thin film should be larger than or equal to that of the 1^{st} layer of IDTs. The "equal" situation is a particular case in which the fabrication is simpler because the final etching step for PAD exposure is not necessary. With these considerations in mind, this part of simulation is based on the structure with the same thickness of SiO_2 and the 1^{st} layer of IDTs. The thicknesses of the 1^{st} layer and the 2^{nd} layer of IDTs are 0.1λ and 0.02λ, respectively,

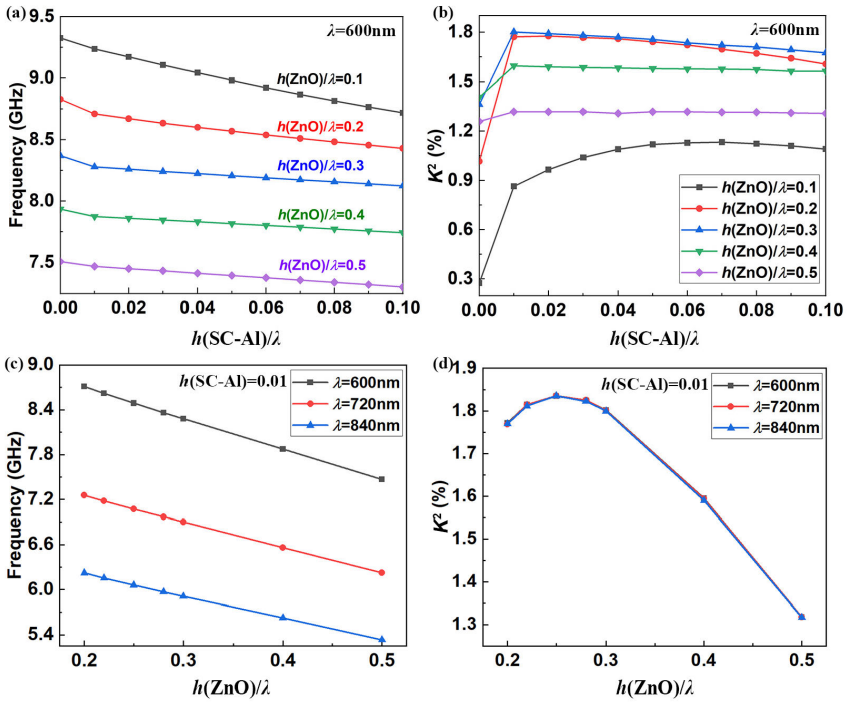

FIGURE 5. Frequency (a, c) and K^2 (b, d) in the second structure as functions of (a, b) the thicknesses of SC-Al and ZnO, (c, d) the thickness of ZnO and the wavelength.

to neutralize the effect from perpendicular component of the electric field. This work also investigates how adding a layer of short-circuit aluminum metal (SC-Al) under the ZnO thin film influences the values of f and K^2. [45]

Fig. 5(a) and 5(b) show the calculated f and K^2 dispersion patterns as functions of h(ZnO)/λ and h(SC-Al)/λ in the structure with g_1 of 50 nm and d of 250 nm. With separately increasing thickness of ZnO and SC-Al, the frequency decreases monotonically, as shown in Fig. 5(a). Fig. 5(b) shows that the value of K^2 increases with the increase of ZnO thickness from 0.1λ to 0.3λ and decreases afterwards. The excitation mechanism of Sezawa mode wave brings this tendency. Similar trend was shown in Reference [34]. Therefore, the optimized thickness of ZnO to achieve a maximum K^2 is suggested to be approximately 0.3λ. Fig. 5(d) shows the more accurate result which is 0.25λ. The short-circuit thin film dramatically improves the value of K^2 and it exhibits a larger dispersion in the structure with thinner ZnO layer. For example, the K^2 of the structure with h(ZnO)/λ of 0.1 is increased from about 0.3% to 1.0%, while the short-circuit thin film is almost useless if h(ZnO)/λ is 0.5. The K^2 of this structure reaches 1.8% when h(ZnO)/λ equals 0.3 and h(SC-Al)/λ equals 0.01.

The calculated f and K^2 as functions of the wavelength and the ZnO thickness are plotted in Fig. 5(c) and 5(d). The curves of λ of 600 nm, 720 nm, 840 nm are the simulation results for the structures with g_1 of 50 nm and d of 250 nm, g_1 of 60 nm and d of 300 nm, g_1 of 70 nm and d of 350 nm, respectively. The value of K^2 doesn't depend on the wavelength, but devices with smaller wavelengths have higher frequencies.

B. SIMULATION OF STRUCTURES BASED ON PIEZOELECTRIC SINGLE CRYSTAL

The third structure is based on piezoelectric single crystal. As mentioned in Section II, in order to ensure the quality of the signal, IDTs need to be modulated properly. In this part of simulation, the 1st layer of IDT is made by Cu and the 2nd layer is made by Al. The corresponding thicknesses are list in Table 1. Only the Al electrode/ SiO_2 (Cu electrode)/ 15°Y-X $LiNbO_3$ substrate structure with the same thickness of the SiO_2 thin film and the 1st layer of IDTs is studied.

Fig. 6(a) and 6(b) show the simulation results of the third structure. When the IDT thickness is increased, the mass load of IDT is larger and the SiO_2 layer is thicker, resulting in the decrease of the values of f and K^2. If the SiO_2 thickness is larger, the distance between the 2nd layer of IDT and the piezoelectric crystal is greater, and the electric field energy inside the piezoelectric layer is reduced. So the value of K^2 which is a factor to measure the transform efficiency of energy decreases. The wavelength influences the frequency but not the K^2. The frequency of this structure with the Cu thickness of 0.05λ is larger than 6.5 GHz and the K^2 is about 4.7%.

The last structure shown in Fig. 1(d) is designed for SAW devices with large bandwidth. The 1st layer of IDTs is embedded into the piezoelectric single crystal and the 2nd layer of IDTs is deposited on the crystal. Without the barrier of the SiO_2 thin film, all the electric field energy is inside the piezoelectric layer and the value of K^2 is much larger, as shown in Fig. 6(d). The two layers of IDTs still need to be designed properly. The materials of IDTs are same as those

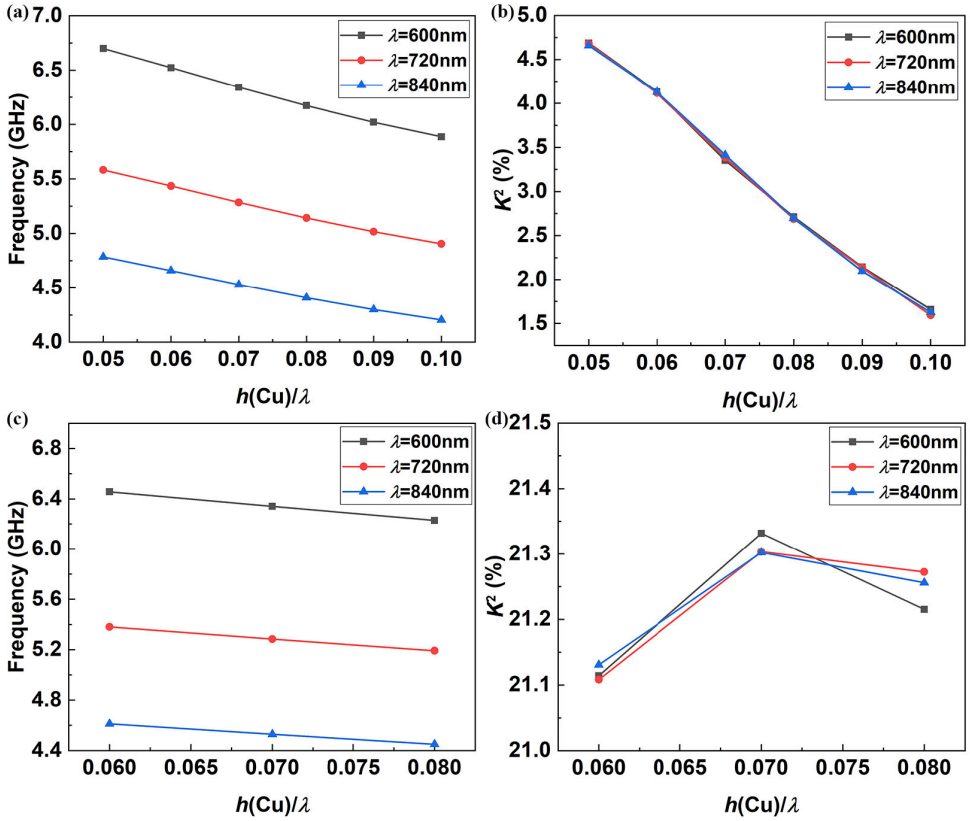

FIGURE 6. Frequency (a, c) and K^2 (b, d) as functions of the thickness of Cu and the wavelength in (a, b) the third structure, (c, d) the fourth structure.

TABLE 1. The thicknesses of two layers of IDTs in the third and the fourth structures.

Structure No.	h(Cu)/λ	h(Al)/λ
3	0.05	0.085
3	0.06	0.092
3	0.07	0.098
3	0.08	0.103
3	0.09	0.107
3	0.10	0.11
4	0.06	0.075
4	0.07	0.083
4	0.08	0.09

of the third structure and the thicknesses are listed in Table 1. The simulation results are plotted in Fig. 6(c) and 6(d). The variation trend and the values of f shown in Fig. 6(c) are similar to those in Fig. 6(a). The values of K^2 in Fig. 6(d) are almost not influenced by the wavelength and the thicknesses of IDTs, and they are much larger than those in Fig. 6(b). The frequency of over 6 GHz and the K^2 over 21% can be achieved by this structure with the wavelength of 600 nm.

C. DISCUSSION

In this paper, a 3D layout of IDTs for high frequency SAW devices is proposed and four structures with the 3D layout of IDTs are designed. The first two structures are based on piezoelectric thin film and the others are based on piezoelectric single crystal.

This 3D layout of IDTs is totally different from conventional layout of IDTs such as the four configurations in Reference [45]. Conventional one layer of IDTs is split into two layers in this work. These two layers of IDTs together form the 3D layout of IDTs. Given certain materials, we have to decrease the sizes of IDT fingers in conventional IDT layout to pursue higher resonant frequency. Eventually the miniature of the pattern would reach the photolithography limit and challenge the current techniques, which is highly unlikely to be addressed within short term. However, by adopting IDTs with a two-layer structure, the distance between adjacent fingers of each layer becomes larger than that in conventional one-layer layout which achieves the same resonant frequency. In other words, we managed to decrease the distance without challenging the current level of photolithography techniques, which means that we are able to further decrease the wavelength and improve the frequency.

When the wavelength of the first two structures (with d of 250 nm and g_1 of 50 nm) is 600 nm, the frequency reaches about 9 GHz. If we take 250 nm as photolithography limit, the minimum wavelength of devices with conventional layout of IDTs can only reach about 1000 nm because the width of each electrode and the gap between adjacent electrodes

both need to be larger than or equal to 250 nm. Compared with the frequency of about 5 GHz which can be achieved by the devices based on Al electrode/ ZnO/ Si substrate with conventional layout of IDTs and wavelength of 1000 nm, this 3D layout of IDTs increases the frequency by about 80%. A challenge to fabricate this 3D layout of IDTs is the overlay accuracy. Taking account of the similar issue on the operation of transverse modes suppression [46]–[48], we believe the fabrication of this 3D layout is still accessible. Compared with the second structure, the first structure has better tolerance for the precision of the overlay exposure because two layers of IDTs can even partially overlap in the vertical direction. As for the second structure, the fabrication techniques are simpler.

Conventional devices based on Cu electrode/ 15°Y-X $LiNbO_3$ and wavelength of 1000 nm have the frequency of about 3 GHz, while the frequency of the latter two structures in this paper with wavelength of 600 nm is higher than 6 GHz. The third structure can exhibit more stable performance under different temperatures in comparison with the fourth structure whose value of K^2 is much larger.

IV. CONCLUSION

In conclusion, a 3D layout of IDTs for the development of high frequency SAW devices is presented by splitting a set of IDTs into two layers, i.e. the ground electrodes on one layer and the signal electrodes on the other layer. This new method dramatically narrows the gap between two adjacent electrodes, which can significantly increase the frequency. Four structures, the first two of which are based on piezoelectric thin film and the last two of which are based on piezoelectric single crystal, are designed to identify the application range of the 3D layout of IDTs. For each structure, one example is chosen to simulate. The four different layered structure, Al electrode/ c-ZnO/ SiO_2(Al electrode)/ Si(100) substrate, Al electrode/ SiO_2(Al electrode)/ c-ZnO/ Si(100) substrate, Al electrode/ SiO_2(Cu electrode)/ 15°Y-X $LiNbO_3$ substrate, Al electrode/ (Cu electrode) 15°Y-X $LiNbO_3$ substrate are modeled, calculated and compared, respectively. By IDT-modulation method, the problem of synchronous bulk wave generation is solved and the signals are as great as conventional SAW devices. The simulation proves that the frequency can be doubled using this 3D layout of IDTs under the same fabrication techniques. All the four structures are possible to be fabricated under the present available technological conditions and their features can be utilized in different applications. This paper proposes a new idea to apply the SAW devices into the field of high frequency and the application of this 3D layout of IDTs is possible and practical. In the future, different structures with the 3D layout of IDTs can be designed for various requirements of devices, and practical devices based on this type of IDTs can be fabricated and tested to show actual properties. This design may enable the high-frequency application of SAW devices and might be an effective cost-cutting approach for the high frequency devices after more researches and efforts.

REFERENCES

[1] M. Agostini, G. Greco, and M. Cecchini, "Full-SAW microfluidics-based lab-on-a-chip for biosensing," *IEEE Access*, vol. 7, pp. 70901–70909, 2019.

[2] M. E. Morales-Rodríguez, P. C. Joshi, J. R. Humphries, P. L. Fuhr, and T. J. Mcintyre, "Fabrication of low cost surface acoustic wave sensors using direct printing by aerosol inkjet," *IEEE Access*, vol. 6, pp. 20907–20915, 2018.

[3] J.-T. Luo, A.-J. Quan, G.-X. Liang, Z.-H. Zheng, S. Ramadan, C. Fu, H.-L. Li, and Y.-Q. Fu, "Love-mode surface acoustic wave devices based on multilayers of TeO_2/ZnO(11$\bar{2}$0)/Si(100) with high sensitivity and temperature stability," *Ultrasonics*, vol. 75, pp. 63–70, Mar. 2017.

[4] T. Bui, V. Nguyen, S. Vollebregt, B. Morana, H. van Zeijl, T. Chu Duc, and P. M. Sarro, "Effect of droplet shrinking on surface acoustic wave response in microfluidic applications," *Appl. Surf. Sci.*, vol. 426, pp. 253–261, Dec. 2017.

[5] K. Wang, W. Zhou, Z. Lin, F. Cai, F. Li, J. Wu, L. Meng, L. Niu, and H. Zheng, "Sorting of tumour cells in a microfluidic device by multi-stage surface acoustic waves," *Sens. Actuators B, Chem.*, vol. 258, pp. 1174–1183, Apr. 2018.

[6] S. Yang, Y. Ai, Z. Cheng, L. Zhang, L. Jia, B. Dong, B. Zhang, J. Wang, and Y. Zhang, "Method of the out-of-band rejection improvement of the AlN based surface acoustic wave filters," *Ultrasonics*, vol. 91, pp. 30–33, Jan. 2019.

[7] J.-T. Tsai, K.-Y. Chiu, and J.-H. Chou, "Performance prediction and sensitivity analysis of SAW gas sensors," *IEEE Access*, vol. 3, pp. 1614–1619, 2015.

[8] N. F. Naumenko, "High-velocity non-attenuated acoustic waves in $LiTaO_3$/quartz layered substrates for high frequency resonators," *Ultrasonics*, vol. 95, pp. 1–5, May 2019.

[9] A. Kumar, G. Thachil, and S. Dutta, "Ultra high frequency acoustic wave propagation in fully polymer based surface acoustic wave device," *Sens. Actuators A, Phys.*, vol. 292, pp. 52–59, Jun. 2019.

[10] M. Park, J. Wang, R. Dargis, A. Clark, and A. Ansari, "Super high-frequency scandium aluminum nitride crystalline film bulk acoustic resonators," in *Proc. IEEE Int. Ultrason. Symp. (IUS)*, Glasgow, U.K., Oct. 2019, pp. 1689–1692.

[11] H. Campanella, J. A. Plaza, J. Montserrat, A. Uranga, and J. Esteve, "High-frequency sensor technologies for inertial force detection based on thin-film bulk acoustic wave resonators (FBAR)," *Microelectron. Eng.*, vol. 86, nos. 4–6, pp. 1254–1257, Apr. 2009.

[12] K. Umeda, H. Kawamura, M. Takeuchi, and Y. Yoshino, "Characteristics of an AlN-based bulk acoustic wave resonator in the super high frequency range," *Vacuum*, vol. 83, no. 3, pp. 672–674, Oct. 2008.

[13] S. Wang, J. Gao, J. Carlier, P. Campistron, A. Ndieguene, S. Guo, O. B. Matar, D.-C. Dorothee, and B. Nongaillard, "Controlling the transmission of ultrahigh frequency bulk acoustic waves in silicon by 45° mirrors," *Ultrasonics*, vol. 51, no. 5, pp. 532–538, Jul. 2011.

[14] S. Fouladi, J. Wu, Q. Zou, A. Barfknecht, A. Vats, M. Nasresfahani, S. Martin, and D. A. Feld, "FBAR resonators fabricated on insulating substrates with improved RF and nonlinear performance," in *Proc. IEEE Int. Ultrason. Symp. (IUS)*, Glasgow, U.K., Oct. 2019, pp. 88–92.

[15] M. Schaefer, R. Rothemund, and G. Fattinger, "Process and design challenge for SMR-type bulk acoustic wave (BAW) filters at frequencies above 5 GHz," in *Proc. IEEE Int. Ultrason. Symp. (IUS)*, Glasgow, U.K., Oct. 2019, pp. 1696–1699.

[16] S. Yandrapalli, V. Plessky, J. Koskela, V. Yantchev, P. Turner, and L. G. Villanueva, "Analysis of XBAR resonance and higher order spurious modes," in *Proc. IEEE Int. Ultrason. Symp. (IUS)*, Glasgow, U.K., Oct. 2019, pp. 185–188.

[17] J. Koskela, V. P. Plessky, B. A. Willemsen, P. J. Turner, B. Garcia, R. B. Hammond, and N. O. Fenzi, "Fast GPU-assisted FEM simulations of 3D periodic TCSAW, IHP, and XBAR devices," in *Proc. IEEE Int. Ultrason. Symp. (IUS)*, Glasgow, U.K., Oct. 2019, pp. 181–184.

[18] J. Zou, V. Yantchev, F. Iliev, V. Plessky, S. Samadian, R. B. Hammond, and P. J. Turner, "Ultra-Large-Coupling and spurious-free SH0 plate acoustic wave resonators based on thin LiNbO3," *IEEE Trans. Ultrason., Ferroelectr., Freq. Control*, vol. 67, no. 2, pp. 374–386, Feb. 2020.

[19] V. Plessky, S. Yandrapalli, P. J. Turner, L. G. Villanueva, J. Koskela, M. Faizan, A. De Pastina, B. Garcia, J. Costa, and R. B. Hammond, "Laterally excited bulk wave resonators (XBARs) based on thin lithium niobate platelet for 5 GHz and 13 GHz filters," in *IEEE MTT-S Int. Microw. Symp. Dig.*, Boston, MA, USA, Jun. 2019, pp. 512–515.

[20] T. Kimura, M. Omura, Y. Kishimoto, and K. Hashimoto, "Comparative study of acoustic wave devices using thin piezoelectric plates in the 3–5-GHz range," *IEEE Trans. Microw. Theory Techn.*, vol. 67, no. 3, pp. 915–921, Mar. 2019.
[21] J. Zou, J. Liu, and G. Tang, "Transverse spurious mode compensation for AlN Lamb wave resonators," *IEEE Access*, vol. 7, pp. 67059–67067, 2019.
[22] T. Mirea, J. Olivares, M. Clement, and J. Sangrador, "AlN-based solidly mounted resonators at 400°: *In-situ* performance monitoring," in *Proc. IEEE Int. Ultrason. Symp. (IUS)*, Glasgow, U.K., Oct. 2019, pp. 1700–1702.
[23] A. Bogner, H.-J. Timme, R. Bauder, A. Mutzbauer, D. Pichler, M. Krenzer, C. Reccius, R. Weigel, and A. Hagelauer, "Impact of high sc content on crystal morphology and RF performance of sputtered $Al_{1-x}Sc_xN$ SMR BAW," in *Proc. IEEE Int. Ultrason. Symp. (IUS)*, Glasgow, U.K., Oct. 2019, pp. 706–709.
[24] T. Yanagitani and J. Jia, "ScAlN polarization inverted resonators and enhancement of k_t^2 in new YbAlN materials for BAW devices," in *Proc. IEEE Int. Ultrason. Symp. (IUS)*, Glasgow, U.K., Oct. 2019, pp. 894–899.
[25] S. Mertin, C. Nyffeler, T. Makkonen, B. Heinz, A. Mazzalai, T. Schmitz-Kempen, S. Tiedke, T. Pensala, and P. Muralt, "Non-destructive piezoelectric characterisation of Sc doped aluminium nitride thin films at wafer level," in *Proc. IEEE Int. Ultrason. Symp. (IUS)*, Glasgow, U.K., Oct. 2019, pp. 2592–2595.
[26] R. Kihara, S. Takayanagi, and T. Yanagitani, "Effect of negative ions generation from sputtering target on crystalline orientation and k_t^2 of ScAlN thin films," in *Proc. IEEE Int. Ultrason. Symp. (IUS)*, Glasgow, U.K., Oct. 2019, pp. 1120–1123.
[27] C. Masamune and T. Yanagitani, "Ion beam induced a-axis in-plane oriented c-axis oriented AlN thin film growth for high-*Q* BAW resonator application," in *Proc. IEEE Int. Ultrason. Symp. (IUS)*, Glasgow, U.K., Oct. 2019, pp. 1127–1128.
[28] M. Clement, V. Felmetsger, J. Olivares, T. Mirea, and J. Sangrador, "Combined assessment of $Al_{1-x}Sc_xN$ thin films by RBS, XRD, FTIR and BAW frequency response measurements," in *Proc. IEEE Int. Ultrason. Symp. (IUS)*, Glasgow, U.K., Oct. 2019, pp. 720–723.
[29] M. Suzuki and S. Kakio, "Electromechanical coupling coefficient k_t^2 of Cr doped AlN films grown by sputtering deposition," in *Proc. IEEE Int. Ultrason. Symp. (IUS)*, Glasgow, U.K., Oct. 2019, pp. 716–719.
[30] P. Kirsch, M. B. Assouar, O. Elmazria, V. Mortet, and P. Alnot, "5GHz surface acoustic wave devices based on aluminum nitride/diamond layered structure realized using electron beam lithography," *Appl. Phys. Lett.*, vol. 88, no. 22, May 2006, Art. no. 223504.
[31] S. Wu, R. Ro, Z.-X. Lin, and M.-S. Lee, "Rayleigh surface acoustic wave modes of interdigital transducer/(100) AlN/(111) diamond," *J. Appl. Phys.*, vol. 104, no. 6, Sep. 2008, Art. no. 064919.
[32] S. Fu, W. Wang, Q. Li, Z. Lu, Z. Chen, J. Luo, J. Shen, R. Wang, C. Song, F. Zeng, and F. Pan, "High-frequency V-doped ZnO/SiC surface acoustic wave devices with enhanced electromechanical coupling coefficient," *Appl. Phys. Lett.*, vol. 114, no. 11, Mar. 2019, Art. no. 113504.
[33] P. Kirsch, M. B. Assouar, O. Elmazria, V. Mortet, and P. Alnot, "5 GHz surface acoustic wave devices based on aluminum nitride/diamond layered structure realized using electron beam lithography," *Appl. Phys. Lett.*, vol. 88, no. 22, May 2006, Art. no. 223504.
[34] S. Fu, W. Wang, L. Qian, Q. Li, Z. Lu, J. Shen, C. Song, F. Zeng, and F. Pan, "High-frequency surface acoustic wave devices based on ZnO/SiC layered structure," *IEEE Electron Device Lett.*, vol. 40, no. 1, pp. 103–106, Jan. 2019.
[35] N. Naumenko, "$LiNbO_3$ plate bonded to quartz as a substrate for high frequency wideband SAW devices," in *Proc. IEEE Int. Ultrason. Symp. (IUS)*, Glasgow, U.K., Oct. 2019, pp. 1227–1230.
[36] S. Asakawa, J. Mizuno, J. Hayashi, M. Suzuki, S. Kakio, A. Tezuka, H. Kuwae, H. Yokota, T. Yonai, and K. Kishida, "Analysis of longitudinal leaky SAW on $LiNbO_3$ thin plate/amorphous layer/Quartz structure," in *Proc. IEEE Int. Ultrason. Symp. (IUS)*, Oct. 2019, pp. 675–678.
[37] K. Hashimoto, H. Asano, K. Matsuda, N. Yokoyama, T. Omori, M. Yamaguchi, "Wideband Love wave filters operating in GHz range on Cu-grating/rotated-YX-$LiNbO_3$-substrate structure," in *Proc. IEEE Ultrason. Symp.*, Montreal, QC, Canada, Aug. 2004, pp. 1330–1334.
[38] J. Luo, A. Quan, C. Fu, and H. Li, "Shear-horizontal surface acoustic wave characteristics of a (110) ZnO/SiO_2/Si multilayer structure," *J. Alloys Compounds*, vol. 693, pp. 558–564, Feb. 2017.
[39] P. Wu, N. W. Emanetoglu, X. Tong, and Y. Lu, "Temperature compensation of SAW in ZnO/SiO_2/Si structure," in *Proc. IEEE Int. Ultrason. Symp. (IUS)*, Atlanta, GA, USA, Oct. 2001, pp. 211–214.
[40] G. Kovacs, M. Anhorn, H. E. Engan, G. Visintini, and C. C. W. Ruppel, "Improved material constants for $LiNbO_3$ and $LiTaO_3$," in *Proc. IEEE Int. Ultrason. Symp. (IUS)*, Honolulu, HI, USA, Dec. 1990, pp. 435–438.
[41] Q.-Z. Zhang, T. Han, W.-B. Wang, K.-Y. Hashimoto, and J. Chen, "Surface acoustic wave propagation characteristics of ScAlN/diamond structure with buried electrode," in *Proc. Symp. Piezoelectricity, Acoustic Waves, Device Appl.*, Beijing, China, Oct. 2014, pp. 271–274.
[42] T. Takai, H. Iwamoto, Y. Takamine, T. Fuyutsume, T. Nakao, M. Hiramoto, T. Toi, and M. Koshino, "High-performance SAW resonator with simplified $LiTaO_3/SiO_2$ double layer structure on Si substrate," *IEEE Trans. Ultrason., Ferroelectr., Freq. Control*, vol. 66, no. 5, pp. 1006–1013, May 2019.
[43] M. Kadota and S. Tanaka, "Simulation of solidly mounted plate wave resonator with wide bandwidth using 0-th shear horizontal mode in $LiNbO_3$ plate," *Jpn. J. Appl. Phys.*, vol. 54, no. 7S1, p. 07HD09, 2015.
[44] T. Kimura, M. Omura, Y. Kishimoto, and K.-Y. Hashimoto, "Applicability investigation of SAW devices in the 3 to 5 GHz range," in *IEEE MTT-S Int. Microw. Symp. Dig.*, Philadelphia, PA, USA, Jun. 2018, pp. 846–848.
[45] W. R. Smith, "Coupling efficiency estimates for acoustic surface wave excitation with piezoelectric film overlays," *J. Appl. Phys.*, vol. 42, no. 7, pp. 3016–3018, Jun. 1971.
[46] M. Solal, O. Holmgren, and K. Kokkonen, "Design, simulation, and visualization of R-SPUDT devices with transverse mode suppression," *IEEE Trans. Ultrason., Ferroelectr., Freq. Control*, vol. 57, no. 2, pp. 412–420, Feb. 2010.
[47] K.-Y. Hashimoto, X. Li, J. Bao, Y. Huang, B. Zhang, and T. Han, "Transverse modes in temperature compensated surface acoustic wave devices," in *Proc. IEEE Int. Ultrason. Symp. (IUS)*, New York, NY, USA, Oct. 2018, pp. 1–9.
[48] M. Solal, J. Gratier, R. Aigner, K. Gamble, B. Abbott, T. Kook, A. Chen, and K. Steiner, "Transverse modes suppression and loss reduction for buried electrodes SAW devices," in *Proc. IEEE Int. Ultrason. Symp.*, San Diego, CA, USA, Oct. 2010, pp. 624–628.

JUNYAO SHEN is currently pursuing the Ph.D. degree with the School of Materials Science and Engineering, Tsinghua University. His research interests include piezoelectric materials, surface acoustic wave (SAW) devices, and lamb wave devices.

JINGTING LUO received the Ph.D. degree from Tsinghua University, Beijing, China, in 2012. Since 2016, he has been an Academic Visitor with the Faculty of Engineering and Environment, University of Northumbria at Newcastle, U.K. He is currently an Associate Professor with the Shenzhen Key Laboratory of Advanced Thin Films and Applications, College of Physics and Optoelectronic Engineering, Shenzhen University, Shenzhen, China.

SULEI FU was born in China, in 1991. He received the Ph.D. degree in material science and engineering from Tsinghua University, China, in 2019. He currently works as a Postdoctoral Fellow at the Key Laboratory of Advanced Materials (MOE), Tsinghua University. His current research interests include simulation and design of various high-performance surface acoustic wave (SAW) devices, piezoelectric materials, and lamb wave devices.

RONGXUAN SU is currently pursuing the Ph.D. degree with the School of Materials Science and Engineering, Tsinghua University. His research interests include FBAR/BAW/SAW devices, piezoelectric materials, and lamb wave devices.

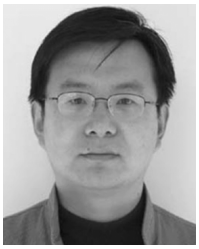

WEIBIAO WANG was born in May 1970. He received the B.Sc. degree from Nanjing Normal University, Nanjing, China, in 1991, and the M.Sc. and Ph.D. degrees from Nanjing University, Nanjing, China, in 2001 and 2005, respectively. He worked as a Postdoctoral Fellow at the State Key Laboratory on Modern Acoustics, Nanjing University, from 2005 to 2006. In 2007, he joined the R&D Team of Shoulder Limited, Wuxi, China, His current interests involve the modeling, simulation, and designing of SAW components.

FEI ZENG received the Ph.D. degree from Tsinghua University, Beijing, China, in 2002. He is currently an Associate Professor with the School of Materials Science and Engineering, Tsinghua University. His current research interests include materials and devices for brain-like computing, such as memristor and artificial neural fibers, as well as surface acoustic wave materials and devices. He has explored elementary materials and individual devices mimicking synaptic plasticity and computing, and has been involved in the research of SAW devices for many years.

CHENG SONG (Member, IEEE) received the Ph.D. degree from Tsinghua University, Beijing, China, in 2009. From 2009 to 2011, he was a Humboldt Research Fellow with the University of Regensburg, Germany. He is currently an Associate Professor with the School of Materials Science and Engineering, Tsinghua University. His research interests are spintronic materials and devices (antiferromagnetic materials, spin-orbit torques, and voltage control of magnetism), as well as resistive switching materials and devices.

FENG PAN received the Ph.D. degree from Tsinghua University, Beijing, China, in 1993. He is currently a Full Professor with the School of Materials Science and Engineering, Tsinghua University. He has coauthored over 300 articles in various domains. His research interests include surface acoustic wave materials and devices, spintronic materials and devices, resistive switching materials and devices, as well as brain-like computing materials and devices.